Available online at www.sciencedirect.com
ScienceDirect
Ceramics International 37 (2011) 1345–1351
CERAMICS INTERNATIONAL
www.elsevier.com/locate/ceramint

On the spinel formation in $Co_{1-x}O/Co_2TiO_4$ composites via reactive sintering, exsolution and oxidation

Kuo-Cheng Yang [1], Pouyan Shen *

Department of Materials and Optoelectronic Science, National Sun Yat-sen University, Kaohsiung, Taiwan, ROC

Received 5 November 2010; received in revised form 18 November 2010; accepted 14 December 2010
Available online 21 January 2011

Abstract

The formation mechanism and microstructural development of the spinel phases in the $Co_{1-x}O/Co_2TiO_4$ composites upon reactive sintering the $Co_{1-x}O$ and TiO_2 powders (9:1 molar ratio) at 1450 °C and during subsequent cooling in air were studied by X-ray diffraction and analytical electron microscopy. The Co_2TiO_4 spinel occurred as inter- and intragranular particles in the matrix of Ti-doped $Co_{1-x}O$ grains with a rock salt-type structure during reactive sintering. The submicron sized Co_2TiO_4 particles were able to detach from grain boundaries in order to reach an energetically favorable parallel orientation with respect to the host $Co_{1-x}O$ grains via a Brownian-type rotation/coalescence process. Upon cooling in air, secondary Co_2TiO_4 nanoparticles were precipitated and the Ti-doped $Co_{1-x}O$ host was partially oxidized as $Co_{3-\delta}O_4$ spinel by rapid diffusion along the {1 1 1} and {1 0 0}-decorated interphase interface and the free surface of the composites.

Keywords: A. Firing; B. Defects; B. Impurities; Cobalt oxides

1. Introduction

The formation mechanism and microstructural development of spinel phases in oxide composites prepared by a sintering route are of concern to their engineering applications. In binary oxide systems with considerable solid solubility, the spinel can be formed by solid-state precipitation from a protoxide of rock salt-type structure or alternatively by reactive sintering of the end members. For example, in the $NiO/NiAl_2O_4$ composite prepared by reactive sintering NiO and Al_2O_3 powders with a negligible extent of nonstoichiometry, the $NiAl_2O_4$ spinel was found to precipitate as micron-sized plates having {1 0 0} habit plane and parallel epitaxial relationship with the rock-salt type host, i.e. Al^{3+}-doped NiO [1]. The $NiAl_2O_4$ spinel also occurred as equi-axed particles, which tended to detach from grain boundaries in order to reach parallel epitaxial relationship with respect to the host via a Brownian-type rotation/coalescence process of the confined particles at high temperature [2]. In binary transition metal oxide systems with rather limited solid solubility yet with varied charges of cations, it is of interest to know whether or not the spinel can be precipitation/oxidation tailored as nanoparticles from the protoxides, besides the formation of much larger sized inter- and intragranular particles via a reactive sintering route.

Here, the $Co_{1-x}O$–TiO_2 binary having the protoxide $Co_{1-x}O$ and the Co_2TiO_4 spinel with negligible mutual solid solubility [3] was chosen for the study. By careful scrutiny of phases and microstructures in the $Co_{1-x}O/Co_2TiO_4$ composites prepared by a reactive sintering route from the $Co_{1-x}O$ and TiO_2 powders, the combined effects of Ti^{4+} exsolution and cobalt oxidation to form spinel nanoparticles from the protoxide $Co_{1-x}O$ upon cooling in air were clarified. We focused also on the reorientation of the inter- and intragranular Co_2TiO_4 spinel particles via a Brownian-type rotation/coalescence process analogous to the cases in other ceramic composites prepared via a solid-state sintering route [2,4–8] or oxidation decomposition route [9].

2. Experimental

CoO (Cerac, 99.5%) and TiO_2 (Aldrich, 99.9%) powders 9:1 in molar ratio were mixed by a magnetic stirrer in ethanol at

* Corresponding author. Fax: +886 7 5254099.
E-mail address: pshen@mail.nsysu.edu.tw (P. Shen).
[1] Present address: Steel and Aluminium R&D Department, China Steel Corporation, Kaohsiung, Taiwan, ROC.

0272-8842/$36.00
doi:10.1016/j.ceramint.2010.12.011

50 °C for 2 h followed by drying at 70 °C and grinding with an agate mortar and pestle. The powder mixture thus prepared was dry-pressed at 650 MPa into pellets ca. 5 mm in diameter and 2 mm in thickness. The pellets were then reactively sintered at 1450 °C for 0.5 h and 4 h followed by quenching in air.

The phases of the as-fired samples were studied by X-ray diffraction (XRD, CuKα, 40 kV, 30 mA, SIEMENS D5000) with a step scanning of 0.05° and fixed counts of 3 s per step in the 2θ range of 15–110°. Lattice parameters of the crystalline phases were determined by least squares fit using the computer software. The deviation of lattice parameters was determined as ±0.0002 nm.

The fired composites were polished and then thermally etched at 1300 °C for 5 min to reveal the grain boundaries using a scanning electron microscope (SEM, 20 kV, JSM-6400, JEOL) under back-scattered electron image (BEI) mode. Energy dispersive X-ray (EDX) analysis was used to analyze the composition of the co-existing phases.

The thin sections of the fired pellets were argon-ion milled to electron transparency and studied by analytical electron microscopy (AEM) using JEOL 3010 instrument at 300 kV for imaging and EDX analysis. The K-shell counts of Co and Ti without absorption correction [10] were used for the semi-quantitative determination of composition at the scale of individual grains. Bright field image (BFI), dark field image (DFI), lattice image and selected area electron diffraction (SAED) taken by transmission electron microscopy (TEM) were used to identify the phases.

3. Results

3.1. XRD

XRD traces (Fig. 1) indicated that the composite fired at 1450 °C for 0.5 h consists of Ti-doped $Co_{1-x}O$ protoxide, $Co_{3-\delta}O_4$ spinel and Co_2TiO_4 spinel with room temperature lattice parameters of 0.4259, 0.8073 and 0.8417 ± 0.0002 nm, respectively. The cell parameters are significantly smaller than the undoped cases, i.e., 0.4260 nm for $Co_{1-x}O$ (JCPDS#09-0402), 0.8084 nm for $Co_{3-\delta}O_4$ (JCPDS#42-1467) and 0.8435 nm for Co_2TiO_4 (JCPDS#39-1410), respectively, indicating a considerable extent of dissolution of smaller-size Ti^{4+} in the phases. The Ti-doped $Co_{1-x}O$, $Co_{3-\delta}O_4$ and Co_2TiO_4 showed little change of lattice parameters upon further aging at 1450 °C for a total of 4 h (Fig. 1).

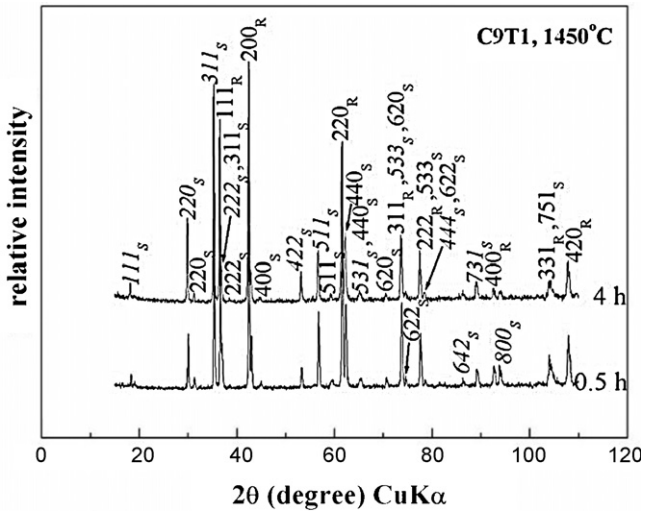

Fig. 1. XRD traces of the samples reaction sintered at 1450 °C for 0.5 h and 4 h followed by air-quenching to room temperature showing the rock-salt structure peaks of $Co_{1-x}O$ (denoted as $(h\,k\,l)_R$), $Co_{3-\delta}O_4$ (denoted as $(h\,k\,l)_S$) and Co_2TiO_4 (denoted as italic $(h\,k\,l)_S$).

3.2. SEM

The specimen reaction-sintered at 1450 °C for 0.5 h showed triple grain junctions characteristic to solid-state sintering despite the presence of intergranular pores (Fig. 2a). The composite actually consists of inter- and intragranular (smaller-sized) Co_2TiO_4 spinel, which gave darker contrast than the host $Co_{1-x}O$ grains in BEI mode. A longer firing time (4 h) at 1450 °C resulted in more intergranular pores and caused considerable coarsening and coalescence of the $Co_{1-x}O$ grains up to ca. 20 μm in diameter according to BEI in Fig. 2b. The size of the intergranular Co_2TiO_4,

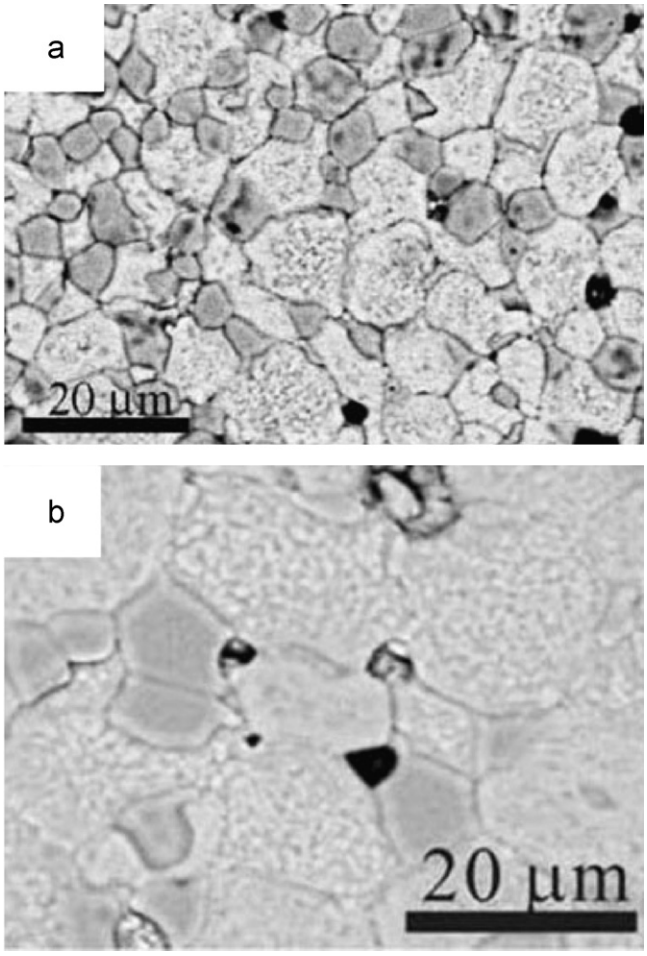

Fig. 2. SEM BEI of the composites fired at 1450 °C for (a) 0.5 h and (b) 4 h showing microstructures characteristic to solid-state sintering, intergranular pores and the Co_2TiO_4 (gray) and $Co_{1-x}O$ (bright) grains.

however, remained almost unchanged upon firing from 0.5 to 4 h at 1450 °C.

3.3. AEM

AEM observations indicated the phase and microstructures of the spinel phases are basically the same in the fired composites although the Ti-doped $Co_{1-x}O$ grains became larger in size when fired from 0.5 to 4 h. The representative observations of inter- and intragranular Co_2TiO_4 particles, secondary Co_2TiO_4 and $Co_{3-\delta}O_4$ precipitates and the semicoherency of the $Co_2TiO_4/Co_{1-x}O$ interface are addressed in turn.

3.3.1. Inter- versus intragranular Co_2TiO_4 particles

The intergranular Co_2TiO_4 spinel is nonepitaxial with respect to the neighboring $Co_{1-x}O$ grains and nearly stoichiometric in composition (Supplement 1), regardless of firing time at 1450 °C.

The relative smaller sized Co_2TiO_4 particles were commonly swept by the grain boundaries of $Co_{1-x}O$ to become intragranular array, as shown by BFI and DFI in Fig. 3a and b, respectively. SAED (Fig. 3c) indicated that such intragranular Co_2TiO_4 spinel particles have reached parallel epitaxy relationship with the host protoxide grain. The Co_2TiO_4 and $Co_{1-x}O$ phases were more or less superimposed as indicated by Moiré fringes in the image (cf. Supplement 2). Point count EDX analysis on the $Co_{1-x}O$ matrix (cf. Supplement 2) showed a slight Ti counts and predominant Co counts. The intragranular Co_2TiO_4 spinel did not show appreciable extent of nonstoichiometry (cf. Supplement 2). The intragranular Co_2TiO_4 particles tended to cluster and coalesce in a parallel epitaxy manner with the $Co_{1-x}O$ host grain as indicated by the representative DFI and SAED pattern in Fig. 4.

3.3.2. Secondary Co_2TiO_4 and $Co_{3-\delta}O_4$ precipitates

The secondary Co_2TiO_4 precipitates remained nanosize and hardly impinged with each other when the composite was subject to firing from 0.5 to 4 h at 1450 °C, as indicated by DFI and corresponding SAED pattern in Fig. 5a and b, respectively. Thus, the Co_2TiO_4 nanoparticles were mostly precipitated during cooling from 1450 °C.

The secondary $Co_{3-\delta}O_4$ precipitates also occurred near the free surface and interphase interface of the composites according to careful scrutiny of the nearly superimposed spinel diffractions with the intragranular Co_2TiO_4 particles and secondary Co_2TiO_4 nanoparticles in [1 1 0] zone axis (Fig. 6). In such a complicated case, the intragranular Co_2TiO_4 and the secondary $Co_2TiO_4/Co_{3-\delta}O_4$ precipitates can still be identified to have been nucleated at tangled dislocations for parallel epitaxy with respect to the $Co_{1-x}O$ grain and the magnified SAED pattern shows nearly superimposed {3 3 3} diffractions of Co_2TiO_4 spinel and $Co_{3-\delta}O_4$ spinel.

3.3.3. Semicoherency of the $Co_2TiO_4/Co_{1-x}O$ interface

The concentration profiles across the intragranular Co_2TiO_4 spinel (Fig. 7a and b) showed that the Co and Ti counts are compensating across the semi-coherent $Co_{1-x}O/Co_2TiO_4$ interface. Lattice image indicates this intragranular Co_2TiO_4 spinel has well-developed {1 1 1} faces and {1 0 0} ledges (Fig. 7c). The reconstructed image (Fig. 7d) showed dislocations, which have half plane parallel to the (0 0 1) near the interface and parallel to the {0 0 1} and {1 1 1} of $Co_{1-x}O$ away from the interface.

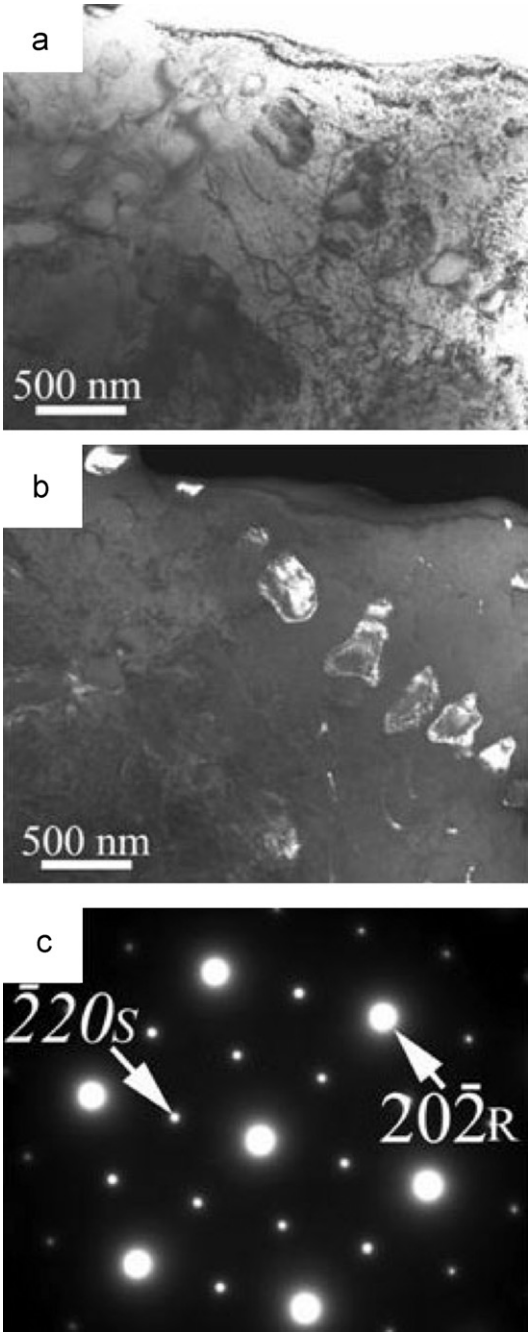

Fig. 3. TEM (a) BFI, (b) DFI ($g = \bar{2}02$) of intragranular Co_2TiO_4 particles in a $Co_{1-x}O$ grain, and (c) SAED pattern of Co_2TiO_4 spinel (denoted as italic *S*) and rock salt-type (denoted as *R*) host grain in [1 1 1] zone axis showing the intragranular Co_2TiO_4 particles have reached a parallel epitaxial relationship with the $Co_{1-x}O$ grain. Sample fired at 1450 °C for 0.5 h and then air quenched to room temperature.

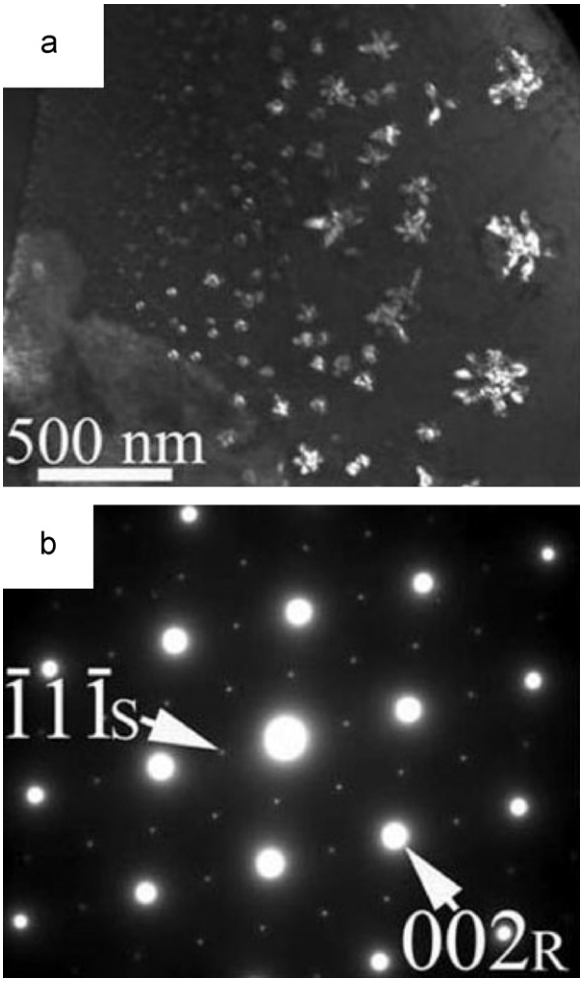

Fig. 4. TEM (a) DFI ($g = 2\bar{2}0$ of spinel) and (b) corresponding SAED pattern in [1 1 0] zone axis of the clustered and coalesced intragranular Co_2TiO_4 particles which are in parallel epitaxy with the $Co_{1-x}O$ host. Sample fired at 1450 °C for 0.5 h and then air quenched to room temperature.

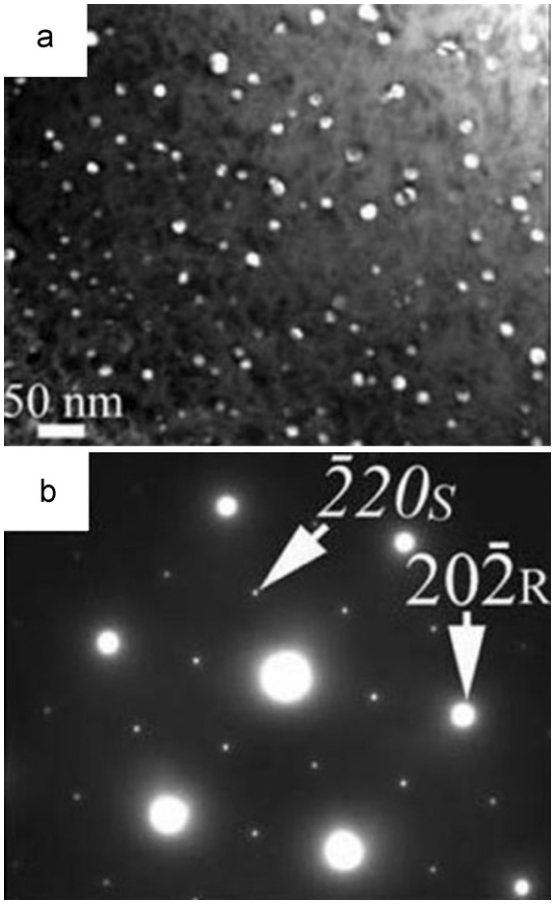

Fig. 5. TEM (a) DFI ($g = 0\bar{2}2$) of secondary and nanosized Co_2TiO_4 precipitates in $Co_{1-x}O$ grain, (b) corresponding SAED pattern in [1 1 1] zone axis, showing the Co_2TiO_4 precipitates seldom impinge with each other. Sample fired at 1450 °C for 4 h and then air quenched to room temperature.

4. Discussion

4.1. Defect chemistry of Ti^{4+}-doped $Co_{1-x}O$

The Ti^{4+} dopant in $Co_{1-x}O$ is expected to cause charge-compensating defect clusters $[V''_{CO} + Co_{Co}^{\bullet}]$ through the following equation in Kröger–Vink notation [11]:

$$TiO_2 \xrightarrow{CoO} Ti_{Co}^{\bullet\bullet} + 2\left[V''_{Co} + Co_{Co}^{\bullet}\right] + 2O_{O^x} \quad (1)$$

Here $Ti_{Co}^{\bullet\bullet}$ signifies dominating double positively charged titanium at cobalt sites in the crystal lattice. A smaller X-ray lattice parameter for Ti-doped $Co_{1-x}O$ (0.4258 nm) than undoped $Co_{1-x}O$ (0.4260 nm) indicates that Ti^{4+} (effective ionic radii, 0.0605 nm) replaced a larger sized Co^{2+} (0.0745 nm and 0.065 nm for high spin and low spin, respectively) in coordination number 6 [12]. It is also possible that the volume-compensating effect, due to the undersized Ti^{4+} dopant in the Co^{2+} site, forced $Co_{Co}^{\bullet}$ to enter the interstitial tetrahedral site, i.e. $Co_i^{\bullet\bullet\bullet}$, and hence more charge-compensating cation vacancies through the following equation:

$$Ti_{CO}^{\bullet\bullet} + [V''_{CO} + Co_{Co}^{\bullet}] \rightarrow Ti_{Co}^{\bullet\bullet} + [Co_i^{\bullet\bullet\bullet} + 4V''_{CO} + 4Co_{Co}^{\bullet}] \quad (2)$$

It remains to be clarified whether the defect clustering scheme of Ti^{4+}-doped $Co_{1-x}O$ involves the 4:1 clusters; the 6:2 clusters composed of two 4:1 clusters with a common edge; and then a paracrystalline state, as the precursor of spinel phase, having cations ordered in the tetrahedral and octahedral sites, analogous to undoped cobalt oxide [13] and Zr^{4+}-doped $Co_{1-x}O$ [14].

4.2. $T-P_{O_2}$ and near-surface effects on the formation of $Co_{3-\delta}O_4$ spinel

Temperature dependent P_{O_2} in atmosphere accounts for the oxidation of bulk and undoped $Co_{1-x}O$ to form $Co_{3-\delta}O_4$ spinel below 900 °C [15]. Cobalt vacancies (V''_{CO}), interstitials ($Co_i^{\bullet\bullet\bullet}$), and 4:1 clusters ($Co_i^{\bullet\bullet\bullet} + 4V''_{Co} + 4Co_{Co}^{\bullet}$) in undoped $Co_{1-x}O$ were suggested to develop into paracrystal and then $Co_{3-\delta}O_4$ spinel, also with paracrystalline distribution of defect clusters [13]. In fact, in

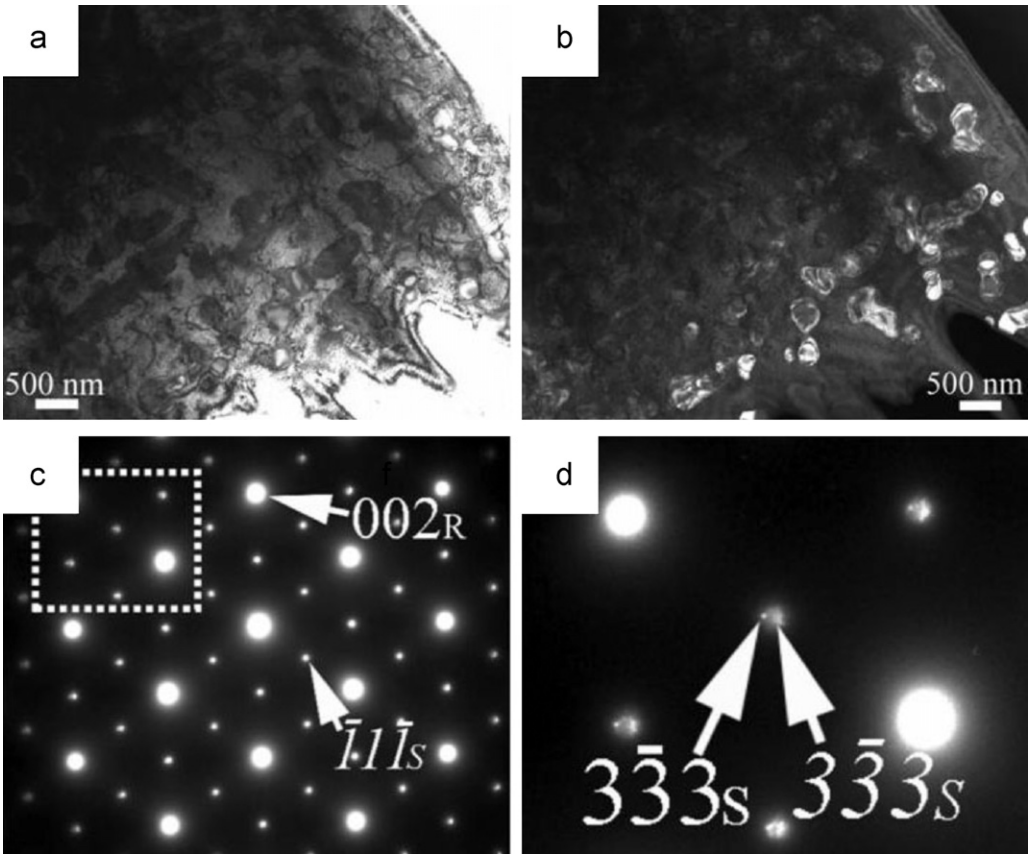

Fig. 6. TEM (a) BFI, (b) DFI ($g = 1\bar{1}\bar{1}$ of Co_2TiO_4 and $Co_{3-\delta}O_4$ spinel), and (c) corresponding SAED pattern in [1 1 0] zone axis showing the intragranular Co_2TiO_4 and the secondary $Co_2TiO_4/Co_{3-\delta}O_4$ precipitates nucleated at dislocations are parallel epitaxial with respect to the $Co_{1-x}O$ grain (d) SAED pattern further magnified from the square region in (c) showing nearly superimposed {3 3 3} diffractions of Co_2TiO_4 spinel (denoted as italic *S*) and $Co_{3-\delta}O_4$ spinel (denoted as *S*). Sample fired at 1450 °C for 4 h and then air quenched to room temperature.

situ work function measurements of the $Co_{1-x}O$ single crystal cleavage in the temperature range 790–905 °C at oxygen partial pressures near the equilibrium with $Co_{3-\delta}O_4$ indicated that the formation and ionization of cobalt vacancies is much faster than the formation of the $Co_i^{\bullet\bullet\bullet}$ donors [16]. These intrinsic defects preferred to occur at free surface and therefore the $Co_{3-\delta}O_4$ structure forms within the near-surface layer under $T-P_{O_2}$ conditions, which correspond to the stability of the CoO phase in the bulk [16]. In view of near-surface $Co_{1-x}O/Co_{3-\delta}O_4$ phase diagram [16], the nucleation of $Co_{3-\delta}O_4$ spinel from the sintered $Co_{1-x}O$ polycrystals could possibly start above 900 °C upon cooling in atmosphere. Spinel nucleation is expected to occur at the free surface of the sintered pellet as well as at dislocations where intrinsic defects segregate and short-circuit diffusion prevails. The $Co_{3-\delta}O_4$ was indeed found to form dominantly on the free surface of the sintered $Co_{1-x}O/Co_2TiO_4$ composites. This was indicated by its preferred occurrence in unpolished sample (according to XRD) rather than Ar-ion thinned TEM foils. It is also possible that the faceted/ledged interface of $Co_{1-x}O$ and Co_2TiO_4 help the nucleation of some $Co_{3-\delta}O_4$ domains in the bulk composite via short circuit oxidation upon cooling in air.

4.3. Heterogeneous nucleation and growth of nano-sized Co_2TiO_4 precipitates

In our previous study of MgO/Mg_2TiO_4 composite, nanosize precipitates of Mg_2TiO_4 spinel were found to precipitate from Guinier–Preston (G.P.) zones in Ti-doped MgO upon cooling [17]. In the present case of less stoichiometric $Co_{1-x}O/Co_2TiO_4$ composite, the Co_2TiO_4 spinel was found to nucleate at dislocations, rather than G.P. zones. Such dislocations could be generated by sintering/coalescence process analogous to the case of nanocrystalline titania [18]. Dislocation cores, having a relatively more open structure than the lattice, are favorable in minimizing the lattice misfit strain energy, and hence lowering the activation energy of nucleation. The dislocations/fault across and near the $Co_{1-x}O/Co_2TiO_4$ interface may act as a source of cobalt vacancies, hence facilitating the formation of 4:1 clusters and ultimately Co_3O_4 spinel nuclei. Unlike $Co_{1-x}O$ [13], and Zr-doped $Co_{1-x}O$ [14], which have the 4:1 defect clusters arranged as a paracrystalline state before transforming into the spinel phase, the present Ti^{4+}-doped $Co_{1-x}O$ transforms directly into the Co_2TiO_4 spinel phase upon cooling. It is not clear whether the dopant dependence of binding energy, the correlation factor, or the migration energy terms affect the

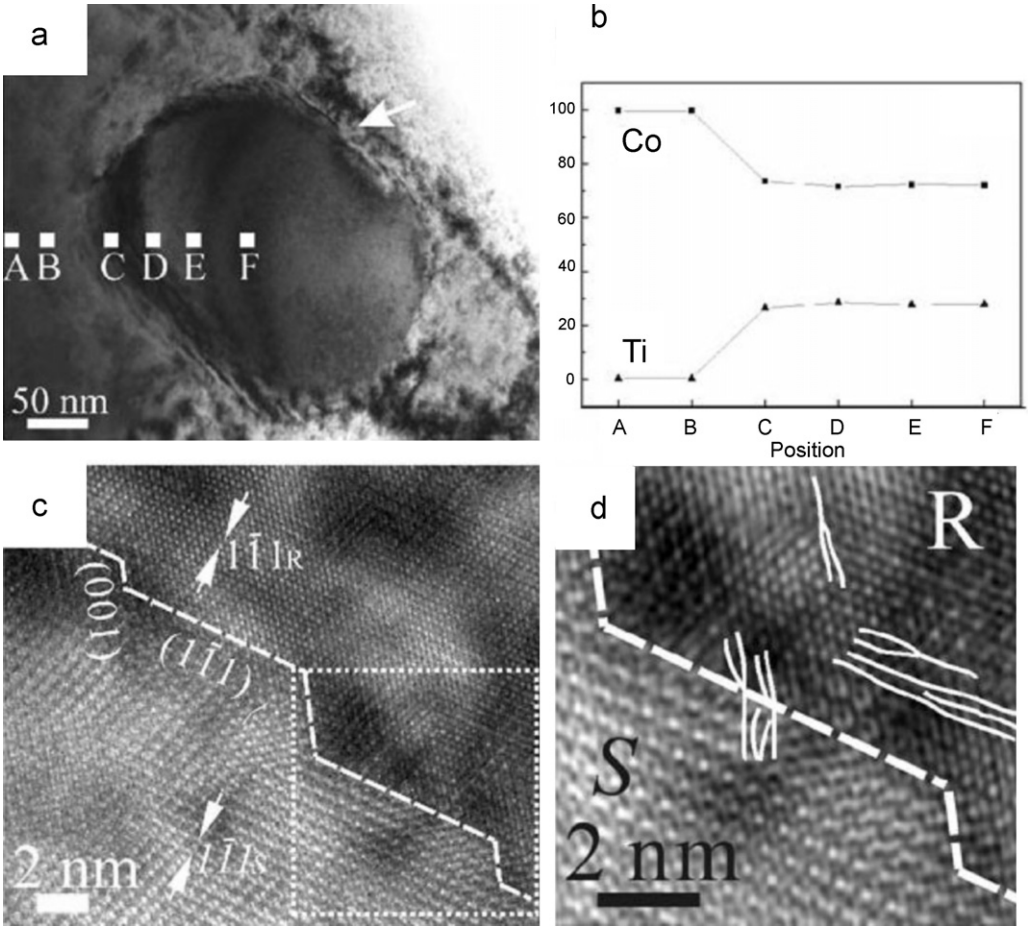

Fig. 7. TEM (a) BFI in [1 1 0] zone axis, (b) EDX composition profile (A–F) across the interface of Co_2TiO_4/Ti-doped $Co_{1-x}O$ in (a), (c) Lattice image from the area denoted by an arrow in (a) showing {1 1 1} and {0 0 1} interfaces (denoted by dashed lines), (d) two-dimensional Fourier-transform from the square region in (c) showing dislocations/fault (delineated by solid lines) near the interface of Co_2TiO_4 spinel (denoted as italic *S*) and Ti-doped $Co_{1-x}O$ matrix (denoted as *R*). Sample fired at 1450 °C for 4 h and then air quenched to room temperature.

transformation route. The Co_2TiO_4 precipitates remained nanosize and seldom impinge with each other in the $Co_{1-x}O$ grain because of a rather limited extent of Ti^{4+} expulsion for precipitate growth.

4.4. Reorientation of intragranular Co_2TiO_4 spinel particles

The intragranular Co_2TiO_4 spinel particles were always in parallel epitaxial orientation with respect to the host $Co_{1-x}O$ grains when annealed at 1723 K for 0.5–4 h. A rather high homologous temperature ($T/T_m = 0.97$, where $T_m = 1783$ K is the eutectic point [3]) in such case was able to trigger orientation change of the intragranular particles, rather than simply 'mold' particles into a shape that lower the total surface energy. The orientation change of the intergranular particles may be significantly affected by reactive sintering stress, biased diffusion and a grain-boundary dragging effect. However, once incorporated in host grains, the particles could still change orientation until they reached epitaxial relationships with respect to the host grains. Such a reorientation behavior for intragranular particles can be rationalized by Brownian-type rotation of the particles as suggested for a number of ceramic composites prepared via a solid-state sintering route or oxidation decomposition route as mentioned. This mechanism has been operated for the fcc metal crystallites over single crystal substrate under nonconservative condition [19], as overviewed in Ref. [20].

As a final remark, the $Co_{1-x}O/ZrO_2$ interface has important catalytic activity for dehydrogenation [21] and oxidation of propane and CO [22] as an automobile exhaust emission catalyst. The complicated $Co_{1-x}O/Co_2TiO_4$ and $Co_{3-\delta}O/Co_2TiO_4$ interfaces as tailored by the size, spatial distribution and orientation of the spinel phases in the protoxide matrix via a reactive sintering route may have analogous applications.

5. Conclusions

1. The Co_2TiO_4 spinel particles formed by reactive sintering were able to detach from the $Co_{1-x}O$ grain boundaries to reach parallel epitaxial orientation with respect to the host $Co_{1-x}O$ grains.
2. The orientation change of intragranular Co_2TiO_4 particles is in accordance with the mechanism of Brownian-type rotation of particles in terms of a 'viscous' diffusion along the $Co_{1-x}O/Co_2TiO_4$ interface.

3. Nanosize Co_2TiO_4 spinel was precipitated from Ti-doped $Co_{1-x}O$ upon cooling of the reactively sintered $Co_{1-x}O/Co_2TiO_4$ composite due to a rather limited exsolution.
4. The $Co_{3-\delta}O_4$ spinel was also formed on the free surface and the $Co_{1-x}O/Co_2TiO_4$ interface of the composite during its cooling and oxidation in air.

Acknowledgments

Supported by Center for Nanoscience and Nanotechnology at NSYSU and partly by National Science Council, Taiwan, ROC under contract NSC94-2216-E119-005.

Appendix A. Supplementary data

Supplementary data associated with this article can be found, in the online version, at doi:10.1016/j.ceramint.2010.12.011.

References

[1] S.R. Wang, P. Shen, On the spinel precipitation in Al-doped $Ni_{1-x}O$, J. Solid State Chem. 140 (1998) 38–45.
[2] S.R. Wang, P. Shen, Rotation-coalescence of confined particles in $Ni_{1-x}O/NiAl_2O_4$ composites, Mater. Sci. Eng. A 251 (1998) 106–112.
[3] B. Brezny, A. Muan, Phase relations and stabilities of compound in the system CoO–TiO_2, J. Inorg. Nucl. Chem. 31 (1969) 649–655.
[4] J. Chen, P. Shen, On the rotation of nonepitaxy $Ni_{1-x}O$ particles within zirconia grain, Scripta Mater. 37 (1997) 1287–1294.
[5] K.T. Lin, P. Shen, Thermally activated rotation of $Co_{1-x}O$ particles within zirconia, Mater. Sci. Eng. A 270 (1999) 125–132.
[6] M.L. Jeng, P. Shen, Thermally activated rotation of $Ni_{1-x}O$ particles within CaO grains, Mater. Sci. Eng. A 338 (2000) 1–9.
[7] W.H. Lee, P. Shen, Reorientation of intra- and intergranular particles in sintered Y-PSZ/$Co_{1-x}O$ composites, Mater. Sci. Eng. A 338 (2002) 253–258.
[8] J.Y. Wang, P. Shen, (1 1 1)-specific reorientation and shape change of $Co_{1-x}O$ particles within CaO grains, Mater. Sci. Eng. A 359 (2003) 192–197.
[9] M.Y. Li, P. Shen, S.L. Hwang, Oxidation-decomposition facilitated reorientation of nanoparticles in reactively sintered $(Ni_{0.33}Co_{0.67})_{1-\delta}O$ polycrystals, Mater. Sci. Eng. A 343 (2003) 227–234.
[10] D.B. Williams, Practical Analytical Electron Microscopy in Materials Science, Philips Electronic Instruments, Mahwah, 1984, pp. 64–74.
[11] F.A. Kröger, H.J. Vink, Relations between the concentrations of imperfections in crystalline solids, Solid State Phys. 3 (1956) 307–435.
[12] R.D. Shannon, Revised effective ionic radii and systematic studies of interatomic distances in halides and chalcogenides, Acta Cryst. A 32 (1976) 751–767.
[13] W.H. Lee, P. Shen, $Co_{3-\delta}O_4$ paracrystal: 3-D assembly of nano-size defect clusters in spinel lattice, J. Solid State Chem. 177 (2004) 101–108.
[14] K.T. Lin, P. Shen, Interdiffusion-induced phase changes of $Co_{1-x}O$/zirconia composites, J. Solid State Chem. 145 (1999) 739–750.
[15] M. Oku, Y. Sato, In-situ x-ray photoelectron spectroscopic study of the reversible phase transition between CoO and Co_3O_4 in oxygen of 10^{-3} Pa, Appl. Surf. Sci. 55 (1992) 37–41.
[16] J. Nowotny, W. Weppner, M. Sloma, Near-surface defect structure of CoO in the vicinity of the CoO/Co3O4 phase boundary, in: J. Nowotny, W. Weppner (Eds.), Non-Stoichiometric Compounds Surfaces, Grain Boundaries and Structural Defects, Kluwer Academic Publishers, Dordrecht, 1989, pp. 265–277.
[17] K.C. Yang, P. Shen, On the precipitation of coherent spinel nanoparticles in Ti-doped MgO, J. Solid State Chem. 178 (2005) 661–670.
[18] R.L. Penn, J.F. Banfield, Imperfect oriented attachment: dislocation generation in defect-free nanocrystals, Science 281 (1998) 969–971.
[19] J.J. Métois, M. Gauch, A. Masson, R. Kern, Epitaxie: phénomène de postudéation sur l'exemple des couches minces discontinues d'aluminium et d'or sur (1 0 0) KCl, Thin Solid Films 11 (1972) 205–218.
[20] L.Y. Kuo, P. Shen, On the rotation of non-epitaxy crystallites on single crystal substrate, Surf. Sci. 373 (1997) L350–L356.
[21] L.A. Boot, M.H.J.V. Kerkhoffs, B.Th. Van der Linden, A.J. Van Dillen, J.W. Geus, F.R. Van Buren, Preparation, characterization and catalytic testing of cobalt oxide and manganese oxide catalysts supported on zirconia, Appl. Catal. A: Gen. 137 (1996) 69–86.
[22] G. Koyano, H. Watanabe, T. Okuhara, M. Misono, Structure and catalysis of cobalt oxide overlayers prepared on zirconia by low-temperature-plasma oxide, J. Chem. Soc. Faraday Trans. 92 (1996) 3425–3430.